

An analysis of globally connected active rotators with excitatory and inhibitory connections having different time constants using the nonlinear Fokker-Planck equations

Takashi Kanamaru, Masatoshi Sekine

Abstract—The globally connected active rotators with excitatory and inhibitory connections having different time constants under noise are analyzed using the nonlinear Fokker-Planck equation, and their oscillatory phenomena are investigated. Based on numerically calculated bifurcation diagrams, both periodic solutions and chaotic solutions are found. The periodic firings are classified based on the firing period, the coefficient of variation, and the correlation coefficient, and weakly synchronized periodic firings which are often observed in physiological experiments are found. (IEEE Trans. on Neural Networks, vol.15, issue 5 (2004) pp.1009-1017.)

Index Terms—active rotator, nonlinear Fokker-Planck equation, oscillation, synchronization, chaos, weakly synchronized periodic firings, balanced-inhibition

I. INTRODUCTION

Recently, in the brain science, the role of pulses from a single neuron and the correlation among pulse trains from different neurons have been attracting considerable attentions, and their importance in the information processing is emphasized by several authors.

Traditionally, it has been considered that information is coded in the firing rate of each neuron, and a single pulse conveys little information because the behaviors of biological neurons seem to be stochastic. On the other hand, in Refs. [1]–[4], a possibility of the information transfer with precise timings of pulses, namely, a possibility of the temporal coding is argued. The role of a single pulse in the brain function is still controversial, but some experimental and theoretical researches have shown that the timing of the firings of single neurons is reliable for time-varying inputs and it can be a candidate for a carrier of information in the brain [5]–[7]. These researches suggest that theoretical analyses of pulse neural networks are of importance to understand the brain function from the neuronal level [8].

Moreover, in the visual cortex and the hippocampus, many ensembles of neurons show oscillatory behaviors, and when such oscillations exist, the pulse trains of neurons in the ensemble have some degree of correlations (For reviews, see Ref. [9]). It is proposed that such correlative oscillations contribute to the binding of information in the visual cortex and the control of the synaptic plasticity in the hippocampus. And it

is also found that the correlation among neurons in oscillating ensembles sometimes becomes very weak [10]–[12]. In Ref. [10], Gray and Singer reported that they could not observe a rhythmicity in the auto-correlation function of the multiunit activity (16 out of 30 cases) even when the local-field potential shows oscillation (29 out of 30) in the cat visual cortex. This experimental result suggests that the degree of synchronization among neurons is very weak, but their collective activity shows an oscillation. Such weakly synchronized periodic firings are also found in the hippocampus [11], [12]. This ubiquity of the weakly synchronized periodic firings might suggest their importance in the information processing in the brain.

Synchronization in neural systems is first modeled by the networks of excitatory neurons [13]–[17], and the transition from the asynchronous state to the synchronous state is analyzed theoretically. Excitatory networks typically yield very fast and highly synchronized periodic firings, thus they might not be able to model synchronized oscillations with relatively small frequencies (*e.g.*, 40 Hz) nor weakly synchronized periodic firings. To model such slow and weakly synchronized periodic firings, the roles of inhibitory neurons might be important, and, recently, the networks composed of excitatory and inhibitory neurons are considered by many researchers [18]–[23]. In our previous study [23], a noisy pulse neural network composed of globally connected excitatory and inhibitory neurons is treated, and various synchronized oscillations including chaotic ones are analyzed. The period of the synchronized periodic firing is determined by the noise intensity and the coupling strength, and, when the system is close to the saddle-node on limit cycle bifurcation, the period becomes very long. However, the degree of synchronization among neurons is somewhat strong, thus this network could not model the weakly synchronized periodic firings.

In the present paper, behaviors of a noisy pulse neural network composed of globally connected excitatory and inhibitory neurons are analyzed with the nonlinear Fokker-Planck equation. With the analyses of the Fokker-Planck equation, the structure of the bifurcations which yield various synchronized firings can be understood. In the previous study [23], it was assumed that the excitatory and inhibitory neurons have identical properties. On the other hand, in the present paper, the time constant of the inhibitory neurons is set twice as that of the excitatory ones to incorporate the experimental observations that the time constant of the inhibitory post-

synaptic potential is longer than that of the excitatory postsynaptic potential [3], [24].

In Section II, the definition of our model is given and its Fokker-Planck equations are introduced. In Section III, the Fokker-Planck equations are analyzed numerically, and bifurcation diagrams are obtained. Both periodic solutions and chaotic solutions are found in some parameter range. The chaotic solutions are analyzed with the Poincaré section and the largest Lyapunov exponent. In Section IV, the pulse trains of the model are analyzed using the interspike interval, the coefficients of variation, and the correlation coefficients. The weakly synchronized periodic firings which are often observed in physiological experiments are also found. Conclusions and discussions are presented in the final section.

II. DEFINITION OF THE MODEL

Let us consider globally connected active rotators composed of excitatory neurons $\theta_E^{(i)}$ ($i = 1, 2, \dots, N_E$) and inhibitory neurons $\theta_I^{(i)}$ ($i = 1, 2, \dots, N_I$) written as

$$\begin{aligned} \tau_E \dot{\theta}_E^{(i)} &= 1 - a \sin \theta_E^{(i)} + \xi_E^{(i)}(t) \\ &+ \frac{g_{EE}}{N_E} \sum_{j=1}^{N_E} (-\sin \theta_E^{(j)} + 1/a) \\ &- \frac{g_{EI}}{N_I} \sum_{j=1}^{N_I} (-\sin \theta_I^{(j)} + 1/a), \end{aligned} \quad (1)$$

$$\begin{aligned} \tau_I \dot{\theta}_I^{(i)} &= 1 - a \sin \theta_I^{(i)} + \xi_I^{(i)}(t) \\ &+ \frac{g_{IE}}{N_E} \sum_{j=1}^{N_E} (-\sin \theta_E^{(j)} + 1/a) \\ &- \frac{g_{II}}{N_I} \sum_{j=1}^{N_I} (-\sin \theta_I^{(j)} + 1/a), \end{aligned} \quad (2)$$

$$\langle \xi_E^{(i)}(t) \xi_E^{(j)}(t') \rangle = D \delta_{ij} \delta(t - t'), \quad (3)$$

$$\langle \xi_I^{(i)}(t) \xi_I^{(j)}(t') \rangle = D \delta_{ij} \delta(t - t'), \quad (4)$$

$$\langle \xi_E^{(i)}(t) \xi_I^{(j)}(t') \rangle = 0, \quad (5)$$

where a is a system parameter and $\xi_E^{(i)}(t)$ and $\xi_I^{(i)}(t)$ are Gaussian white noises with the intensity D injected to the neurons $\theta_E^{(i)}$ and $\theta_I^{(i)}$, respectively. And τ_E and τ_I are the time constants. Note that the active rotator is a general model of the class 1 neuron [25], [26]. For $a > 1$, an active rotator shows typical properties of an excitable system, namely, it has a stable equilibrium $\theta_0 \equiv \arcsin(1/a)$ and $-\sin(\theta^{(i)}(t)) + 1/a$ shows a pulse-like waveform with an appropriate amount of disturbance. When a is close to 1, the equilibrium θ_0 is close to $\pi/2$. In the following, we only consider excitable, not self-oscillating neurons. Although the active rotators are often connected diffusively [27]–[30], the active rotators in our model are connected with the term $-\sin(\theta^{(i)}(t)) + 1/a$ to imitate the synaptic connections in the brain.

Let us define the normalized number density of rotators

having the phase θ_E and θ_I at time t as

$$n_E(\theta_E, t) \equiv \frac{1}{N_E} \sum_{i=1}^{N_E} \delta(\theta_E^{(i)} - \theta_E), \quad (6)$$

$$n_I(\theta_I, t) \equiv \frac{1}{N_I} \sum_{i=1}^{N_I} \delta(\theta_I^{(i)} - \theta_I), \quad (7)$$

for the excitatory neurons and inhibitory neurons, respectively. With $n_E(\theta_E, t)$ and $n_I(\theta_I, t)$, (1) and (2) are rewritten as

$$\begin{aligned} \tau_E \dot{\theta}_E^{(i)} &= 1 - a \sin \theta_E^{(i)} + \xi_E^{(i)}(t) \\ &+ g_{EE} \int_0^{2\pi} d\phi_E (-\sin \phi_E + 1/a) n_E(\phi_E, t) \\ &- g_{EI} \int_0^{2\pi} d\phi_I (-\sin \phi_I + 1/a) n_I(\phi_I, t), \end{aligned} \quad (8)$$

$$\begin{aligned} \tau_I \dot{\theta}_I^{(i)} &= 1 - a \sin \theta_I^{(i)} + \xi_I^{(i)}(t) \\ &+ g_{IE} \int_0^{2\pi} d\phi_E (-\sin \phi_E + 1/a) n_E(\phi_E, t) \\ &- g_{II} \int_0^{2\pi} d\phi_I (-\sin \phi_I + 1/a) n_I(\phi_I, t). \end{aligned} \quad (9)$$

In the limit of $N_E, N_I \rightarrow \infty$, $n_E(\theta_E, t)$ and $n_I(\theta_I, t)$ may be identified with the probability densities. With this approximation, $n_E(\theta_E, t)$ and $n_I(\theta_I, t)$ follow the nonlinear Fokker-Planck equation [31], [32] written as

$$\frac{\partial n_E}{\partial t} = -\frac{1}{\tau_E} \frac{\partial}{\partial \theta_E} (A_E n_E) + \frac{D}{2\tau_E^2} \frac{\partial^2 n_E}{\partial \theta_E^2}, \quad (10)$$

$$\frac{\partial n_I}{\partial t} = -\frac{1}{\tau_I} \frac{\partial}{\partial \theta_I} (A_I n_I) + \frac{D}{2\tau_I^2} \frac{\partial^2 n_I}{\partial \theta_I^2}, \quad (11)$$

$$\begin{aligned} A_E(\theta_E, t) &= 1 - a \sin \theta_E \\ &+ g_{EE} \int_0^{2\pi} d\phi_E (-\sin \phi_E + 1/a) n_E(\phi_E, t) \\ &- g_{EI} \int_0^{2\pi} d\phi_I (-\sin \phi_I + 1/a) n_I(\phi_I, t), \end{aligned} \quad (12)$$

$$\begin{aligned} A_I(\theta_I, t) &= 1 - a \sin \theta_I \\ &+ g_{IE} \int_0^{2\pi} d\phi_E (-\sin \phi_E + 1/a) n_E(\phi_E, t) \\ &- g_{II} \int_0^{2\pi} d\phi_I (-\sin \phi_I + 1/a) n_I(\phi_I, t). \end{aligned} \quad (13)$$

If there are no correlations among the firings of neurons, n_E and n_I converge to stationary densities, and if some correlation exists, n_E and n_I have time-varying densities. In the limit of $N_E, N_I \rightarrow \infty$, the dynamics of neurons can be followed by solving (8) and (9) together with the nonlinear Fokker-Planck equations (10) and (11) for a desired number of neurons, and we call it an infinite system. With the infinite system, we can investigate the interspike interval and the coefficient of variation of each neuron, and the correlation between two pulse trains from two neurons in the system.

For simplicity, the connection coefficients are set as $g_{EE} = g_{II} \equiv g_{int}$ and $g_{IE} = g_{EI} \equiv g_{ext}$, and the parameters are set as $a = 1.05$, $g_{int} = 1.0$, $\tau_E = 1$, and $\tau_I = 2$. Note that the system with $\tau_E = \tau_I = 1$ is treated in Ref. [23], and several oscillatory behaviors including chaotic ones are

observed. Here we treat the system with $\tau_E = 1$ and $\tau_I = 2$ to incorporate the experimental observations that the time constant of the inhibitory post-synaptic potential is longer than that of the excitatory post-synaptic potential [3], [24].

Similar to the results in Ref. [23], numerical solutions of the Fokker-Planck equations with uniform initial conditions $n_E = n_I = 1/2\pi$ show various behaviors depending on the noise intensity D and the connection strength g_{ext} . The typical shapes of n_E and n_I , and the corresponding firing patterns for $\tau_E = \tau_I = 1$ are shown in Ref. [23]. Here we briefly summarize the behaviors of the system with $\tau_E = 1$ and $\tau_I = 2$. Typically, for small D , all neurons emit spikes randomly with small firing rates, thus n_E and n_I are sharply peaked at their equilibria. When D is large, the excitatory neurons start to fire almost periodically with large firing rates, but those firings do not have correlations, thus the system has stable stationary probability densities. And when the noise intensity D and the connection strength g_{ext} are appropriately chosen, all the neurons oscillate with some correlations, and the probability densities n_E and n_I also oscillate periodically. In the following, we call the firings which correspond to the time-varying solutions of n_E and n_I as synchronized firings.

In the next section, the mechanism of the emergence of synchronized firings is analyzed.

III. BIFURCATION ANALYSIS

Numerically calculated bifurcation diagrams in the (D, g_{ext}) plane are shown in Figs. 1 (a) and (b). The solid, dotted, and dash-dotted lines denote the Hopf, saddle-node, and global bifurcations, respectively. Typically, there exist synchronized firings in the area between the Hopf bifurcation line and the saddle-node on limit cycle bifurcation line with moderate values of D . In Fig. 1, flows in the plane of probability fluxes J_E and J_I are also shown, and their explanations are given in the latter half of this section.

The Hopf and saddle-node bifurcation lines are obtained as follows. First, (6) and (7) are 2π -periodic functions of θ_E and θ_I , respectively, thus they can be expanded as

$$n_E(\theta_E, t) = \frac{1}{2\pi} + \sum_{k=1}^{\infty} (a_k^E(t) \cos(k\theta_E) + b_k^E(t) \sin(k\theta_E)),$$

$$n_I(\theta_I, t) = \frac{1}{2\pi} + \sum_{k=1}^{\infty} (a_k^I(t) \cos(k\theta_I) + b_k^I(t) \sin(k\theta_I)),$$

and, by substituting them, (10) and (11) are transformed into a set of ordinary differential equations $\dot{\mathbf{x}} = \mathbf{f}(\mathbf{x})$ where $\mathbf{x} = (a_1^E, b_1^E, a_1^I, b_1^I, a_2^E, b_2^E, a_2^I, b_2^I, \dots)^t$. Next a stationary solution \mathbf{x}_0 is numerically obtained with the Newton method [33], and the eigenvalues of the Jacobian matrix $D\mathbf{f}(\mathbf{x}_0)$ are analyzed numerically using the QR algorithm [33]. For numerical calculations, the dimension of \mathbf{x} is set 160 or 240 depending on the parameters D and g_{ext} .

To understand the bifurcation diagram in Fig. 1, let us introduce the probability fluxes [34] $J_E(\theta_E, t)$ and $J_I(\theta_I, t)$

written as

$$J_E(\theta_E, t) = \frac{1}{\tau_E} A_E n_E - \frac{D}{2\tau_E^2} \frac{\partial n_E}{\partial \theta_E}, \quad (16)$$

$$J_I(\theta_I, t) = \frac{1}{\tau_I} A_I n_I - \frac{D}{2\tau_I^2} \frac{\partial n_I}{\partial \theta_I}. \quad (17)$$

In the following, the fluxes at $\theta_E = \theta_I = 3/2\pi$ are observed because they can be interpreted as the instantaneous firing rate at t for each ensemble. Note that a stationary solution and an oscillating solution of the Fokker-Planck equation are projected as an equilibrium point and a limit cycle onto the (J_E, J_I) plane, respectively.

Schematic flows in the (J_E, J_I) plane for $1.2 < g_{ext} < 2.5$ are also shown in Fig. 1 (a). Typically, there are three equilibrium points S_0, S_1 and S_2 which satisfy $J_E \sim J_I \sim 0$, $J_E > J_I$, and $J_I > J_E$, respectively, and a limit cycle L_1 is formed around S_1 . S_0 and S_1 are stable for small and large D , respectively. Note that the limit cycle L_1 corresponds to the synchronized firings, and it is created around S_1 by the Hopf bifurcation, the saddle-node on limit cycle bifurcation, or the homoclinic bifurcation. The Hopf, saddle-node, and homoclinic bifurcation lines intersect at a single point like the Bogdanov-Takens bifurcation [35]. The trajectory at the homoclinic bifurcation line is shown in the inset (1) in Fig. 1 (a) where the unstable manifold of the unstable equilibrium spirals back to the identical point. Such a trajectory is possible because this dynamics actually has infinite degrees of freedom. For further information of each bifurcation, see Refs. [35], [36].

Schematic flows in the (J_E, J_I) plane for $0.2 < g_{ext} < 0.8$ are shown in Fig. 1 (b). Typically, two equilibrium points S_0, S_1 , and the limit cycle L_1 around S_1 exist. Although S_1 appears to exist outside of L_1 in the (J_E, J_I) plane, this is because the high-dimensional dynamics is projected onto the two-dimensional plane, and the trajectory from the initial point near S_1 converges to L_1 as shown in the inset (4) of in Fig. 1 (b). The limit cycle L_1 is created by a double limit cycle (DLC1 in Fig. 1 (b)) bifurcation, namely, the simultaneous emergence of stable and unstable limit cycles. The bifurcation around the DLC1 line becomes complex for $D < 0.03$, and a limit cycle with 2 or more cycles suddenly emerges when crossing the bifurcation line. To analyze this bifurcation, the long computational times and the large numerical precision are required, thus we could not determine its mechanism. Thus this bifurcation is labeled as “unknown” in the inset (5) which shows a schematic bifurcation diagram around the intersection of the saddle-node bifurcation line and the double limit cycle bifurcation line. Although we could not observe the homoclinic bifurcation (HB) in the inset (5) in Fig. 1 (b), it was shown in a broken line as a conjecture. From the schematic flows in the (J_E, J_I) plane, it seems to be natural to assume the existence of such a bifurcation.

Moreover, with the double limit cycle bifurcation denoted as DLC2 in Fig. 1 (b), another limit cycle L_C is created, but we do not draw its schematic trajectory for simplicity. This limit cycle L_C is destabilized by a period doubling bifurcation, and, after a series of period doubling bifurcations, a chaotic solution emerges. In the following, we denote both

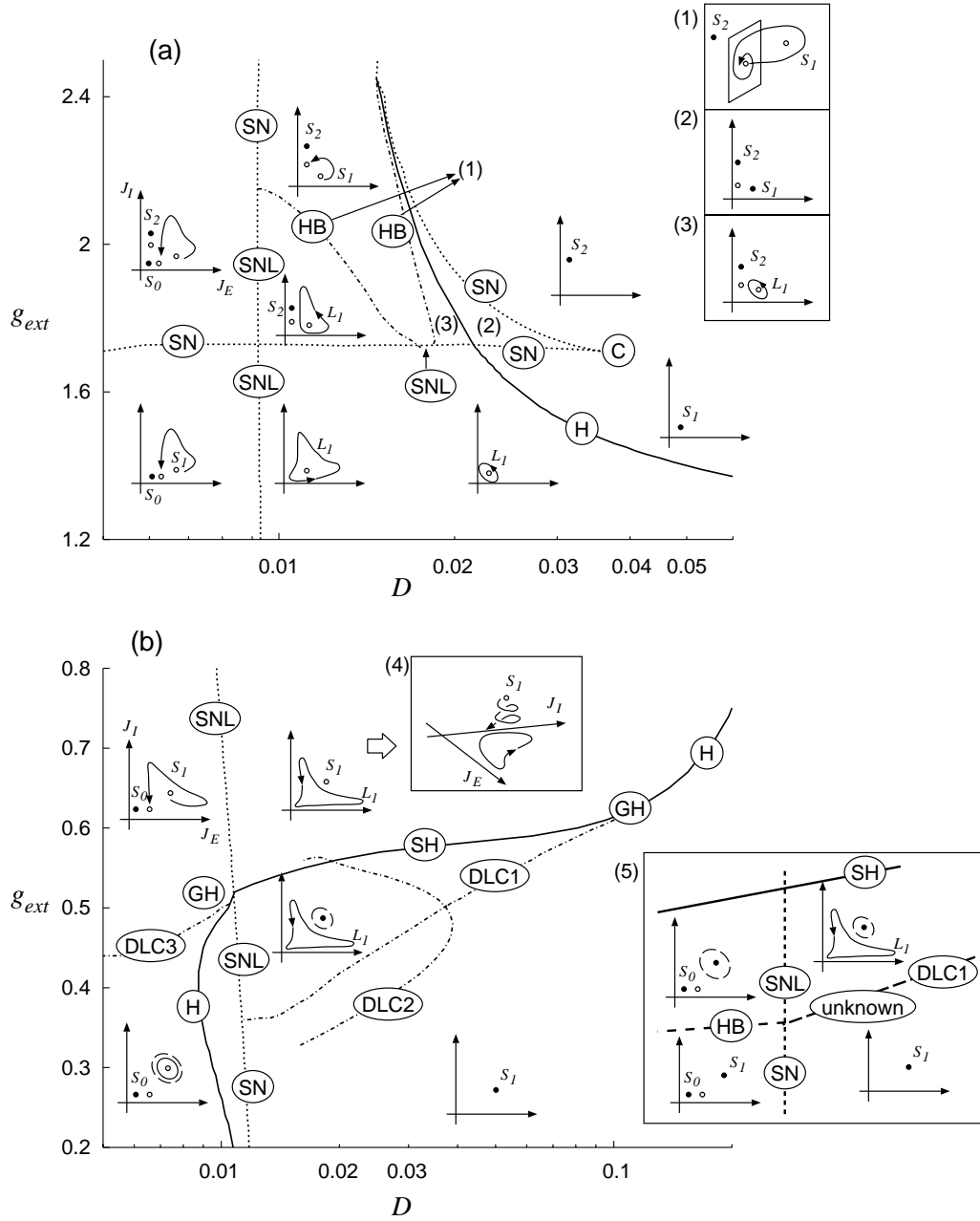


Fig. 1. Numerically calculated bifurcation diagrams for (a) $1.2 < g_{ext} < 2.5$ and for (b) $0.2 < g_{ext} < 0.8$ with the schematic flows in the (J_E, J_I) plane. The solid and dotted lines denote the Hopf bifurcation line and the saddle-node bifurcation line, respectively. The dash-dotted lines denote the global bifurcations. The filled and open circles in the trajectories in the (J_E, J_I) plane denote the stable and unstable equilibrium points, respectively. And the solid and dashed closed curves denote the stable and unstable limit cycle, respectively. The meanings of the abbreviations are as follows: C, Cusp; SN, saddle-node; SNL, saddle-node on limit cycle; HB, homoclinic bifurcation; DLC, double limit cycle; H, Hopf; GH, generalized Hopf; SH, subcritical Hopf.

the periodic solutions and the chaotic solutions as L_C because they originate from the same double limit cycle bifurcation DLC2.

To characterize L_C , let us consider a Poincaré section at the line $J_I = 0.02$ in the (J_E, J_I) plane, and observe the points where the trajectory intersects this line in the positive direction. The positions of the attractors for L_C and L_1 on the Poincaré section against g_{ext} for $D = 0.03$ are shown in Fig. 2 (a). The range of g_{ext} is determined so that it covers the area where L_C exists. It is observed that L_1 and L_C coexist, L_C becomes chaotic through a series of period-

doubling bifurcations, and it disappears by a crisis.

To confirm that the chaotic behaviors in Fig. 2 (a) are actually chaotic, the largest Lyapunov exponent is calculated by a standard technique [37], namely, by calculating the expansion rate of two nearby trajectories each of which follows a set of ordinary differential equations $\dot{x} = f(x)$ for the spatial Fourier coefficients of (10) and (11). In Fig. 2 (b), the largest Lyapunov exponent for L_C corresponding to Fig. 2 (a) is shown. It is observed that it takes positive values when chaotic solutions exist, and takes zero when periodic solutions are stable.

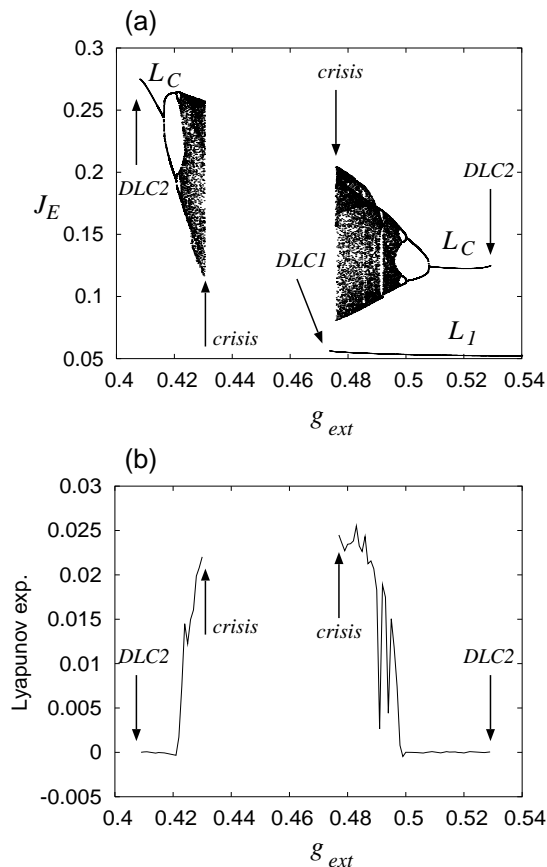


Fig. 2. (a) The bifurcation diagram for $D = 0.03$. The points at which the trajectory crosses the line $J_I = 0.02$ in the positive direction are plotted. (b) The corresponding largest Lyapunov exponent.

IV. PULSE ANALYSIS

In the previous section, the Fokker-Planck equations (10) and (11) are treated, and the average behaviors of neurons are analyzed. The numerically obtained bifurcation diagram is more complex than that of the system with $\tau_E = \tau_I = 1$ treated in the previous study [23], but both mechanisms of bifurcations are similar. In this section, the infinite system governed by (8), (9), (10), and (11) is mainly considered, and the behaviors of a single neuron in the network with infinite number of neurons are investigated. With such analyses, the comparison of our model with the experimental data would become possible, and we would observe the weakly synchronized periodic firings which are not found in the previous study. In the following, the parameters where only the oscillating solution is stable in the system are treated.

First, let us define the interspike interval (ISI) as

$$T_k = t_{k+1} - t_k, \quad (18)$$

where t_k is the k -th firing of the neuron. Note that the firing time of the i -th neuron is defined as the time when $-\sin(\theta^{(i)}(t)) + 1/a$ exceeds the value 1.5. With T_k , the coefficient of variation of the pulse train $\{t_k\}_k$ is defined as

$$C_V = \frac{\sqrt{\langle T_k^2 \rangle - \langle T_k \rangle^2}}{\langle T_k \rangle}. \quad (19)$$

where $\langle \cdot \rangle$ denotes the average over k . C_V takes large values for random pulse trains, and takes zero for periodic pulse trains. The mean interspike interval $T \equiv \langle T_k \rangle$ and C_V are used to investigate the properties of a single pulse train. In the following, the mean interspike intervals and the coefficients of variation of the excitatory and inhibitory neurons are denoted as T_E , T_I , C_{VE} , and C_{VI} , respectively.

Next, let us define the correlation coefficient C between two pulse trains [38]. Usually, the correlation between two phase models is measured by the order parameter $\langle \cos(\theta_i - \theta_j) \rangle$, but it takes large values even when two rotators are fluctuating around their equilibria, thus it is not appropriate to measure the correlation between two pulse trains. To define C , the time under observation is divided into n bins of the width Δ , and the number of pulses in the i -th bin is denoted as X_i and Y_i for two pulse trains. Note that the width Δ is sufficiently small so that X_i and Y_i take the value 0 or 1. Then $X = \sum X_i$ and $Y = \sum Y_i$ are the numbers of pulses, and $Z = \sum X_i Y_i$ is the number of coincident pulses. The correlation coefficient C between two pulse trains is defined as

$$C = \frac{Z - (XY)/n}{\sqrt{X(1 - X/n)Y(1 - Y/n)}} \in [-1, 1]. \quad (20)$$

Note that C takes the value 1 for the identical pulse trains and takes the value 0 in the large n limit for two pulse trains without correlation. And C takes the value -1 when two pulse trains have a negative correlation, namely, $X_i + Y_i = 1$ for $i = 0, 1, 2, \dots$. In the following, the value $\Delta = 5$ is used.

Let us consider two infinite systems, each of which is governed by (8), (9), (10), and (11) with statistically independent noises. This system is composed of two excitatory and two inhibitory neurons, and each neuron is statistically identical with the one in the original system with infinite numbers of neurons. Thus the correlations between two neurons in the infinite system reflect the correlation among the neurons in the original finite system. In the following, the correlations between two excitatory neurons and between two inhibitory neurons are denoted as C_{EE} and C_{II} , respectively.

The dependences of T_E , T_I , C_{VE} , C_{VI} , C_{EE} , and C_{II} on the noise intensity D is shown in Fig. 3 for three values of g_{ext} . In the following, the behaviors of excitatory neurons are mainly considered. For all g_{ext} , near the SNL bifurcation, the periods T and the correlations C take large values, and the coefficients of variation C_V take small values. It is because the system spends a large time around its original equilibrium after the saddle-node bifurcation. Following Ref. [19], let us denote such firings as SSR (slow, synchronous, and regular) firings. Near the Hopf bifurcations, T , C , and C_V take small values for $g_{ext} = 0.7$, and T and C take small values, and C_V takes large values for $g_{ext} = 1.0$. Thus let us denote these firings as FAR (fast, asynchronous, and regular) firings and FAI (fast, asynchronous, and irregular) firings, respectively. Near the Hopf bifurcation for $g_{ext} = 1.5$, the anomalous behavior where T increases with the increase of D is observed. (Fig. 3 (c)). Let us denote such firings as SAI (slow, asynchronous, and irregular) firings.

The raster plots of the firing times of SSR, FAR, FAI, and SAI firings for the finite system with $N_E = N_I = 1000$, and

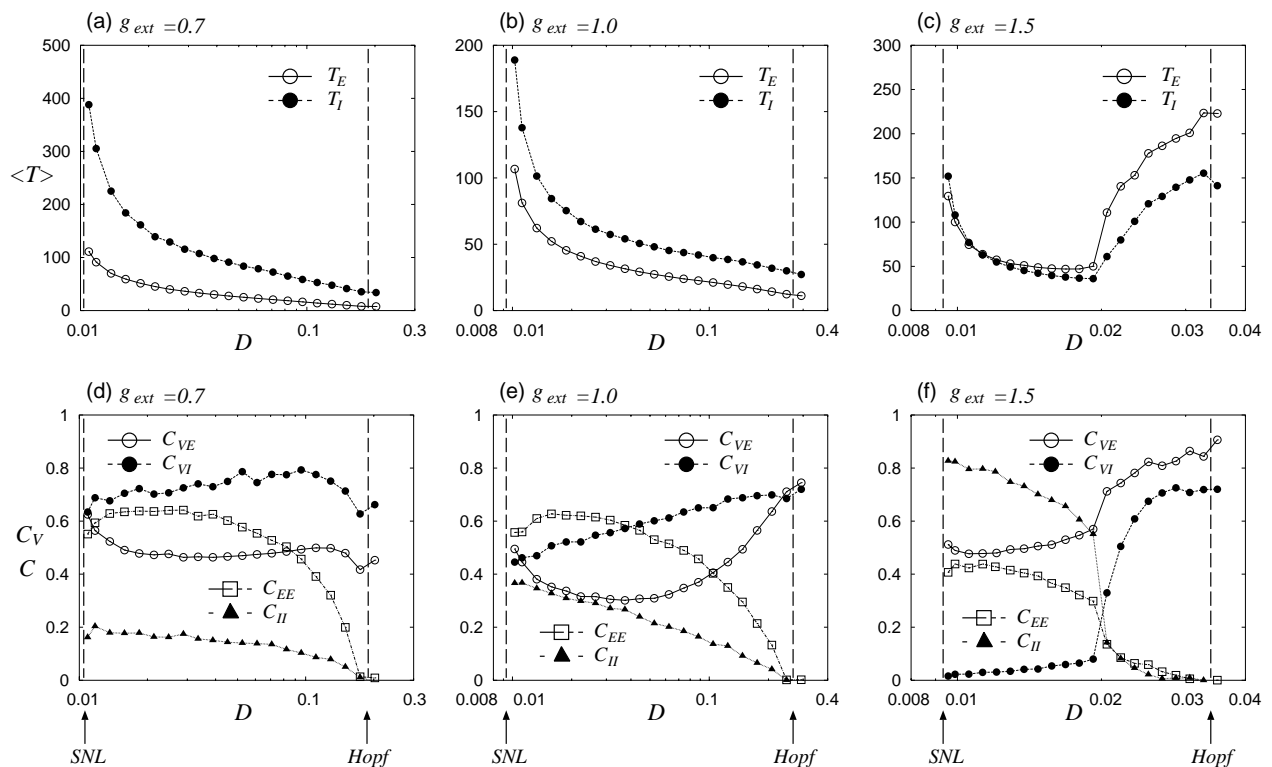


Fig. 3. The dependence of T on D for (a) $g_{ext} = 0.7$, (b) $g_{ext} = 1.0$, and (c) $g_{ext} = 1.5$, and the dependences of C_V and C on D for (d) $g_{ext} = 0.7$, (e) $g_{ext} = 1.0$, and (f) $g_{ext} = 1.5$.

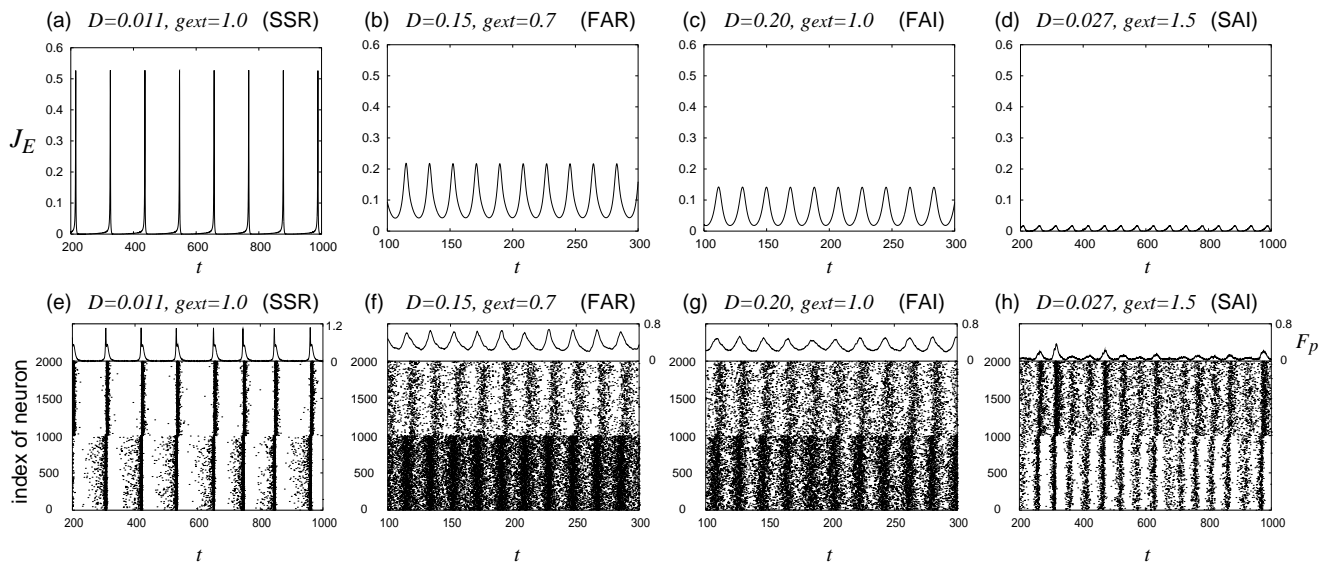


Fig. 4. The probability fluxes of (a) SSR, (b) FAR, (c) FAI, and (d) SAI and the corresponding raster plots of the firing times for the finite system with $N_E = N_I = 1000$. In the raster plot of each firing, the field potential of the excitatory neurons is also shown.

the corresponding probability fluxes are shown in Fig. 4. In the raster plot of each firing, the field potential of the excitatory neurons defined as

$$F_p = \frac{1}{N_E} \sum_{i=1}^{N_E} \left(-\sin(\theta_E^{(i)}(t)) + 1/a \right), \quad (21)$$

is also shown. In the SSR firings (Figs. 4 (a) and (e)), it

is observed that almost all the neurons strongly synchronize each other. In the FAR firings (Figs. 4 (b) and (f)), all the excitatory neurons fire with high frequency, but their degrees of synchronization are weak. The each excitatory neuron fires several times every period (about 15) because the minimum value of J_E is large, thus each neuron tends to fire with the interval of the width of pulse (about 5) and the firings

become relatively regular. In the FAI firings (Figs. 4 (c) and (g)), all the excitatory neurons have high frequencies and weak correlations. However, unlike the FAR firings, the each excitatory neuron fires about once every period (about 20), thus the variance of the ISIs is large, and C_V takes large values. Also in the SAI firings (Figs. 4 (d) and (h)), the correlation among the excitatory neurons is weak, but the SAI firings have an essentially different property from the other firings. The raster plots of SAI firings in Fig. 4 (h) is enlarged in Fig. 5. It is observed that only a small fraction of neurons

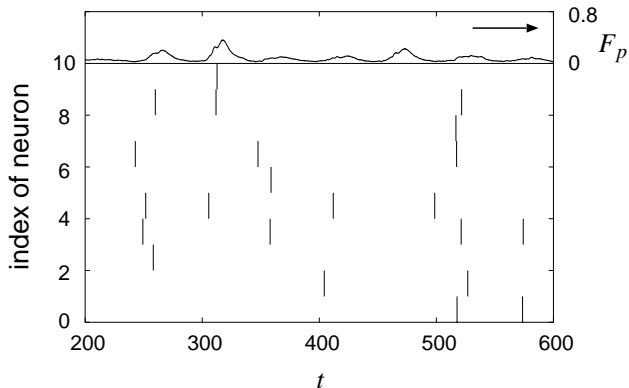


Fig. 5. The enlarged figure of the raster plots of SAI firings in Fig. 4 (h).

fire every period, namely, the periodicity and the degree of synchronization of the SAI firings are very weak.

For each firings, the auto-correlograms defined as a histogram of the difference $t_k - t_l$ ($k, l = 1, 2, \dots$) of the firing times of an excitatory neuron in the finite system with $N_E = N_I = 1000$ are shown in Figs. 6 (a), (b), (c), and (d). The maximum value of the auto-correlogram is normalized to 1. It is observed that the SSR firings have a long period and show a strong periodicity. Moreover, there are long periods of time when almost all the neurons are silent. The FAR firings have a short period, and have peaks at the width of the pulse (about ± 5), and the period of the FAI firings is also short. And it is observed that the periodicity of the SAI firings is very weak.

Similarly, their cross-correlograms are shown in Figs. 6 (e), (f), (g), and (h). The cross-correlogram for two pulse trains $\{t_k^1\}$ and $\{t_l^2\}$ is defined as a histogram of the difference $t_l^2 - t_k^1$ which is normalized by the number of pulses of the pulse train $\{t_k^1\}$, and it is calculated for two neurons in the network. It is observed that the sharp peak at $t = 0$ is observed only for the SSR firings, namely, the degree of synchronization of the SSR firings is stronger than the other firings.

As shown above, the field potential F_p of the SAI firings show a periodicity (Fig. 4 (h)), but the auto-correlogram of a single neuron shows a very weak periodicity. Such weakly synchronized periodic firings are reported in many physiological experiments [10]–[12], and the SAI firings might relate to them. The mechanism of the SAI firings is understood as follows. As shown in (1) and (2), or (8) and (9), the input to a neuron in the network is composed of a sum of mean-field inputs and noise, and when a periodic solution exists in

the system, the mean-field inputs work as a periodic input to the neuron. When this periodic input is sub-threshold for the neuron, the SAI firings take place. Note that the Hopf bifurcation must take place near the origin in the (J_E, J_I) plane to obtain the sub-threshold periodic input (see Figs. 1 (a) and 4 (d)). The boundary of the parameters which yield the SAI firings are shown in Fig. 7. This boundary shows

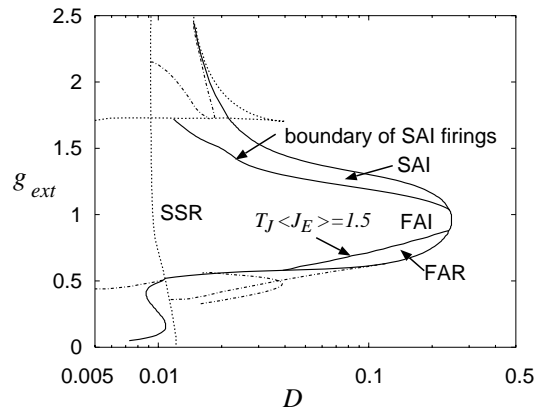


Fig. 7. The boundaries of the FAR, FAI, and SAI firings. The typical areas where each firings take place are also shown.

the parameters where the neuron starts to fire in the system governed by (8), (9), (10), and (11) with $\xi_E^{(i)}(t) = \xi_I^{(i)}(t) = 0$. In the area enclosed by the boundary line, the Hopf bifurcation line, and the saddle-node bifurcation line, only the SAI firings are stable in the system.

The difference between the FAR firings and the FAI firings is the strength of periodicity, and excitatory neurons in the FAR firings tend to fire even when the probability flux J_E is minimum. Thus, for convenience, we define the boundary between the FAR firings and the FAI firings as a line of $T_J \langle J_E(t) \rangle = 1.5$ where T_J is the period of $J_E(t)$ and $\langle \cdot \rangle$ denotes the average over time. Note that $T_J \langle J_E(t) \rangle$ is a mean number of firings in one period T_J of an excitatory neuron. For the neurons in the FAR firings or FAI firings, $T_J \langle J_E(t) \rangle$ tend to be larger than 1 because they fire at least once when $J_E(t)$ is maximum. If $T_J \langle J_E(t) \rangle > 1.5$ is satisfied, the probability for the neuron to fire when J_E is minimum is larger than that to be silent, thus we define such firings as FAR firings. This boundary is also shown in Fig. 7.

V. CONCLUSIONS AND DISCUSSIONS

The globally connected active rotators with excitatory and inhibitory connections having different time constants under noise are analyzed using the nonlinear Fokker-Planck equation, and their oscillatory phenomena are investigated. Based on numerically calculated bifurcation diagrams, the average behavior of the network is analyzed, and both periodic solutions and chaotic solutions are found. The bifurcation diagram is more complex than that of the network with identical time constants ($\tau_E = \tau_I$) [23], but both mechanisms of the bifurcations are similar. When behaviors of a single neuron are observed, the effect of the different time constants becomes clear. The periodic firings are classified based on the statistics obtained

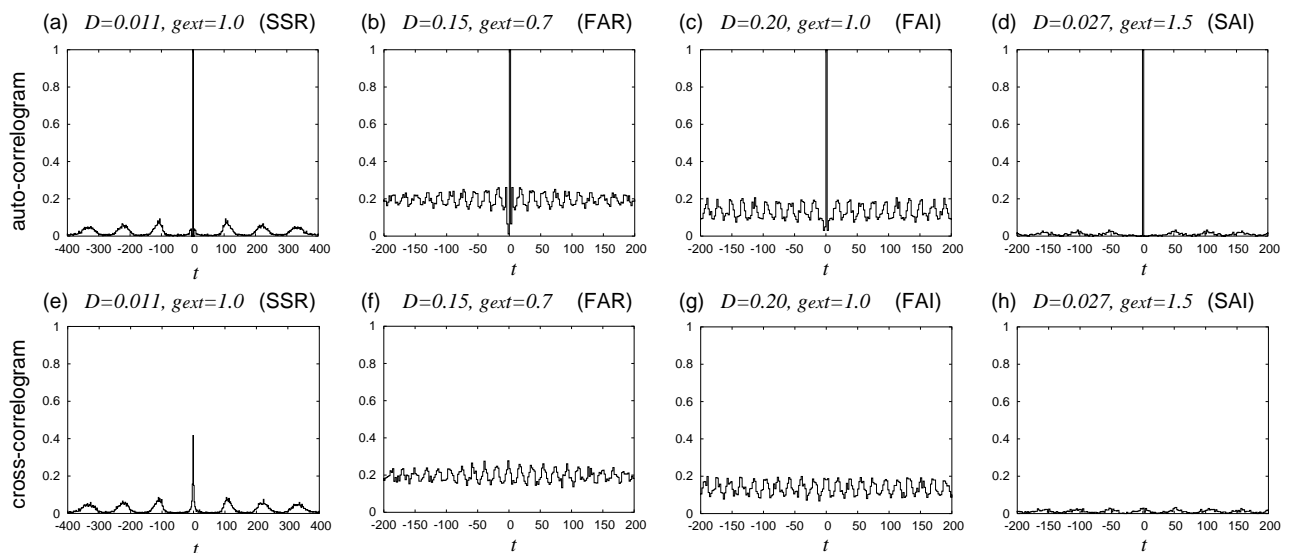


Fig. 6. The auto-correlograms of the firing times of a neuron in the finite system with $N_E = N_I = 1000$ for the (a) SSR, (b) FAR, (c) FAI, and (d) SAI firings, and the corresponding cross-correlograms.

from single neurons, namely, the firing period, the coefficient of variation, and the correlation coefficient. The SSR (slow, synchronous, and regular) firings are observed near the saddle-node bifurcation line, and the FAR (fast, asynchronous, and regular) firings, the FAI (fast, asynchronous, and irregular) firings, and the SAI (slow, asynchronous, and irregular) firings are observed near the Hopf bifurcation line. The periodicity and the degree of synchronization of the SAI firings are very weak, and similar firings are observed in many physiological experiments [10]–[12]. Such weakly synchronized periodic firings are not found in the network with identical time constants. It is found that the SAI firings are caused by a sub-threshold mean-field periodic input and noise. Note that the input composed of a sub-threshold periodic input and noise is often considered in the literature of stochastic resonance [39]. Although the external signal does not exist in our system, the interactions among neurons generate a sub-threshold periodic input. Note that the strength of the periodic input also changes with the change of the noise intensity, thus the theoretical results of stochastic resonance would not apply to our model.

To obtain a sub-threshold periodic input, the Hopf bifurcation must take place near the origin in the (J_E, J_I) plane (see Figs. 1 (a) and 4 (d)). Such a situation would be realized when the firings of excitatory neurons and inhibitory neurons are balanced [2], [18]. In the previous study for $\tau_E = \tau_I = 1$, the SAI firings did not take place because the firing rates of the excitatory neurons are larger than those of inhibitory neurons [23]. On the other hand, for $\tau_E = 1$ and $\tau_I = 2$, the effect of the firings of inhibitory neurons are relatively strengthened because the effect of the inhibition lasts for longer times, thus the balanced state is realized. General conditions to obtain such a balanced state have not been understood, but, under our constraints $g_{EE} = g_{II} = g_{int}$ and $g_{EI} = g_{IE} = g_{ext}$, the time constant of inhibitory neurons must be larger than that of excitatory neurons to realize the balanced state and the weakly

synchronized periodic firings.

Let us interpret the synchronized oscillation from a standpoint of information coding in the brain. A neuron in an oscillating ensemble contributes to the generation of the oscillation, and, for the weakly synchronized periodic firings (SAI firings), this contribution is very weak. This weakness might imply that this neuron can belong to multiple oscillating ensembles with different frequencies simultaneously. If such an oscillating ensemble with weak synchronization is interpreted as a cell assembly and corresponds to a function in the brain [40], [41], a neuron which belongs to multiple oscillating ensembles contributes to different tasks of the brain simultaneously. In this scheme of information coding, the brain performs various tasks with repetitive rearrangements of synchronized ensembles. Examining the possibility of such an information coding from a dynamical standpoint is a future work.

ACKNOWLEDGEMENT

T.K. is grateful to Professor Takehiko Horita for his encouragement. This research was partially supported by a Grant-in-Aid for Encouragement of Young Scientists (B) (No. 14780260) from the Ministry of Education, Culture, Sports, Science, and Technology, Japan.

REFERENCES

- [1] W.R. Softky and C. Koch, “The highly irregular firing of cortical cells is inconsistent with temporal integration of random EPSPs,” *J. Neurosci.*, vol.13, no.1, pp.334–350, 1993.
- [2] M.N. Shadlen and W.T. Newsome, “Noise, neural codes and cortical organization,” *Curr. Opin. Neurobiol.*, vol.4, pp.569–579, 1994.
- [3] W.R. Softky, “Simple codes versus efficient codes,” *Curr. Opin. Neurobiol.*, vol.5, pp.239–247, 1995.
- [4] M.N. Shadlen and W.T. Newsome, “Is there a signal in the noise?,” *Curr. Opin. Neurobiol.*, vol.5, pp.248–250, 1995.
- [5] R.R. de Ruyter van Steveninck, G.D. Lewen, S.P. Strong, R. Koberle, and W. Bialek, “Reproducibility and variability in neural spike trains,” *Science*, vol.275, pp.1805–1808, 1997.

- [6] M.J. Berry, D.K. Warland, and M. Meister, "The structure and precision of retinal spike trains," *Proc. Nat. Acad. Sci. USA*, vol.94, pp.5411–5416, 1997.
- [7] Z.F. Mainen and T.J. Sejnowski, "Reliability of spike timing in neocortical neurons," *Science*, vol.268, pp.1503–1506, 1995.
- [8] *Pulsed Neural Networks*, W. Maass and C.M. Bishop ed., The MIT Press, Cambridge, 1999.
- [9] C.M. Gray, "Synchronous oscillations in neuronal systems: mechanisms and functions," *J. Comput. Neurosci.*, vol.1, pp.11–38, 1994.
- [10] C.M. Gray and W. Singer, "Stimulus-specific neuronal oscillations in orientation columns of cat visual cortex," *Proc. Natl. Acad. Sci. USA*, vol.86, pp.1698–1702, 1989.
- [11] G. Buzsáki, Z. Horváth, R. Urioste, J. Hetke, and K. Wise, "High-frequency network oscillation in the hippocampus," *Science*, vol.256, pp.1025–1027, 1992.
- [12] A. Fisahn, F.G. Pike, E.H. Buhl, and O. Paulsen, "Cholinergic induction of network oscillations at 40Hz in the hippocampus in vitro," *Nature*, vol.394, pp.186–189, 1998.
- [13] R.E. Mirollo and S.H. Strogatz, "Synchronization of pulse-coupled biological oscillators," *SIAM J. Appl. Math.*, vol.50, pp.1645–1662, 1990.
- [14] Y. Kuramoto, "Collective synchronization of pulse-coupled oscillators and excitable units," *Physica D*, vol.50, pp.15–30, 1991.
- [15] M. Tsodyks, I. Mitkov, and H. Sompolinsky, "Pattern of synchrony in inhomogeneous networks of oscillators with pulse interactions," *Phys. Rev. Lett.*, vol.71, pp.1280–1283, 1993.
- [16] L.F. Abbott and C. van Vreeswijk, "Asynchronous states in networks of pulse-coupled oscillators," *Phys. Rev. E*, vol.48, pp.1483–1490, 1993.
- [17] C. van Vreeswijk, "Partial synchronization in populations of pulse-coupled oscillators," *Phys. Rev. E*, vol.54, pp.5522–5537, 1996.
- [18] C. van Vreeswijk and H. Sompolinsky, "Chaos in neuronal networks with balanced excitatory and inhibitory activity," *Science*, vol.274, pp.1724–1726, 1996.
- [19] N. Brunel, "Dynamics of sparsely connected networks of excitatory and inhibitory spiking neurons," *J. Comput. Neurosci.*, vol.8, pp.183–208, 2000.
- [20] D. Golomb and G.B. Ermentrout, "Bistability in pulse propagation in networks of excitatory and inhibitory populations," *Phys. Rev. Lett.*, vol.86, pp.4179–4182, 2001.
- [21] D. Hansel and G. Mato, "Asynchronous states and the emergence of synchrony in large networks of interacting excitatory and inhibitory neurons," *Neural Comput.*, vol.15, pp.1–56, 2002.
- [22] C. Börgers and N. Kopell, "Synchronization in networks of excitatory and inhibitory neurons with sparse, random connectivity," *Neural Comput.*, vol.15, pp.509–538, 2003.
- [23] T. Kanamaru and M. Sekine, "Analysis of the globally connected active rotators with excitatory and inhibitory connections using the Fokker-Planck equation," *Phys. Rev. E*, vol.67, 031916, 2003.
- [24] Ö. Bernander, R.J. Douglas, K.A.C. Martin, and C. Koch, "Synaptic background activity influences spatiotemporal integration in single pyramidal cells," *Proc. Natl. Acad. Sci. USA*, vol.88, pp.11569–11573, 1991.
- [25] B. Ermentrout, "Type I membranes, phase resetting curves, and synchrony," *Neural Comput.*, vol.8, pp.979–1001, 1996.
- [26] E.M. Izhikevich, "Class 1 neural excitability, conventional synapses, weakly connected networks, and mathematical foundations of pulse-coupled models," *IEEE Trans. on Neural Networks*, vol.10, pp.499–507, 1999.
- [27] S. Shinomoto and Y. Kuramoto, "Phase transitions in active rotator systems," *Prog. Theor. Phys.*, vol.75, no.5, pp.1105–1110, 1986.
- [28] H. Sakaguchi, S. Shinomoto, and Y. Kuramoto, "Phase transitions and their bifurcation analysis in a large population of active rotators with mean-field coupling," *Prog. Theor. Phys.*, vol.79, no.3, pp.600–607, 1988.
- [29] C. Kurrer and K. Schulten, "Noise-induced synchronous neuronal oscillations," *Phys. Rev. E*, vol.51, no.6, pp.6213–6218, 1995.
- [30] S. Tanabe, T. Shimokawa, S. Sato, and K. Pakdaman, "Response of coupled noisy excitable systems to weak stimulation," *Phys. Rev. E*, vol.60, no.2, pp.2182–2185, 1999.
- [31] Y. Kuramoto, *Chemical Oscillations, Waves, and Turbulence*, Springer, Berlin, 1984.
- [32] W. Gerstner and W. Kistler, *Spiking Neuron Models*, Cambridge, Cambridge University Press, 2000.
- [33] W.H. Press, B.P. Flannery, S.A. Teukolsky, and W.T. Vetterling, *Numerical Recipes in C*, Cambridge University Press, New York, 1988.
- [34] C.W. Gardiner, *Handbook of Stochastic Methods*, Springer-Verlag, Berlin, 1985.
- [35] F.C. Hoppensteadt and E.M. Izhikevich, *Weakly Connected Neural Networks*, Springer, New York, 1997.
- [36] J. Guckenheimer and P. Holmes, *Nonlinear Oscillations, Dynamical Systems, and Bifurcations of Vector Fields*, Springer, New York, 1983.
- [37] E. Ott, *Chaos in Dynamical Systems*, Cambridge University Press, New York, 1993.
- [38] G. Palm, A.M.H.J. Aertsen, and G.L. Gerstein, "On the significance of correlations among neuronal spike trains," *Biol. Cybern.*, vol.59, pp.1–11, 1988.
- [39] L. Gammitoni, P. Hänggi, P. Jung, and F. Marchesoni, "Stochastic resonance," *Rev. Mod. Phys.*, vol.70, no.1, pp.223–287, 1998.
- [40] D.O. Hebb, *The organization of behavior – a neuropsychological theory*, John Wiley, New York, 1949.
- [41] H. Fujii, H. Ito, K. Aihara, N. Ichinose, and M. Tsukada, "Dynamical cell assembly hypothesis – Theoretical possibility of spatio-temporal coding in the cortex," *Neural Networks*, vol.9, no.8, pp.1303–1350, 1996.

PLACE
PHOTO
HERE

the digital technology.

PLACE
PHOTO
HERE

the digital technology.

Takashi Kanamaru received the B.E. degree in Applied Physics and M.E. degrees in Mathematical Engineering and Information Physics from the University of Tokyo, Tokyo, Japan in 1996 and 1998, respectively. He received D.Eng. from the University of Tokyo in 2001. He is now a research associate in the Department of Electrical and Electronic Engineering, Tokyo University of Agriculture and Technology. His current research interests are the understanding of the dynamics of pulse neural networks and their hardware implementation with

Masatoshi Sekine received the B.S. degree in physics from Tokyo Institute Technology in 1974, the M.S. degree from the University of Tokyo in 1976, and the Ph.D. degree from the University of Tokyo in 1998. Since 1996 till 1999, he has been engaged in Toshiba Research and Development Center, where he has performed and directed bipolar/cmos design, HDL simulator, high level and logic synthesis, neural net and wavelet circuit. From 1992 to 1993 he was a visiting fellow at Electrical Engineering and Computer Science at the University California at Berkeley. In 1999 he joined Tokyo University of Agriculture and Technology as a professor in Electrical and Electronics Engineering. His research interests include reconfigurable systems, circuits for robotics, brain computers, pattern recognition with wavelet transforms, multiscale problems, learning in neural network, and artificial intelligence.